FULL PAPER

Geomagnetic activity dependence and dawn-dusk asymmetry of thermospheric winds from 9-year measurements with a Fabry–Perot interferometer in Tromsø, Norway

Shin-ichiro Oyama[1,2,3*] , Anita Aikio[3], Takeshi Sakanoi[4], Keisuke Hosokawa[5], Heikki Vanhamäki[3], Lei Cai[3], Ilkka Virtanen[3], Marcus Pedersen[3], Kazuo Shiokawa[1], Atsuki Shinbori[1], Nozomu Nishitani[1] and Yasunobu Ogawa[2]

Abstract

Ion drag associated with the ionospheric plasma convection plays an important role in the high-latitude thermospheric dynamics, yet changes in the thermospheric wind with geomagnetic activity are not fully understood. We performed a statistical analysis of the thermospheric wind measurements with a Fabry–Perot interferometer (FPI; 630 nm wavelength) in Tromsø, Norway, in the winter months for 9 years. The measurements were sorted by a SuperMAG (SME) index, and a quiet-time wind pattern was defined as an hourly mean under SME $\leq$ 40 nT. The quiet-time wind pattern can be expected to be represented by a pressure gradient associated with the solar radiation and a geostrophic force balance. With an increase in the geomagnetic activity level, the thermospheric wind turned over from eastward to westward at dusk and increased the equatorward magnitude from midnight to dawn. Deviations from the quiet-time wind presented similar patterns in the direction with the ionospheric plasma convection but were larger in magnitude at dusk than at dawn. This is the first study to report a dawn-dusk asymmetry of the thermospheric wind acceleration feature and signatures of the eastward wind acceleration at dawn by ion drag.

Keywords Ionosphere, Thermosphere, Ion drag, High latitude, Fabry–Perot interferometer, Aurora
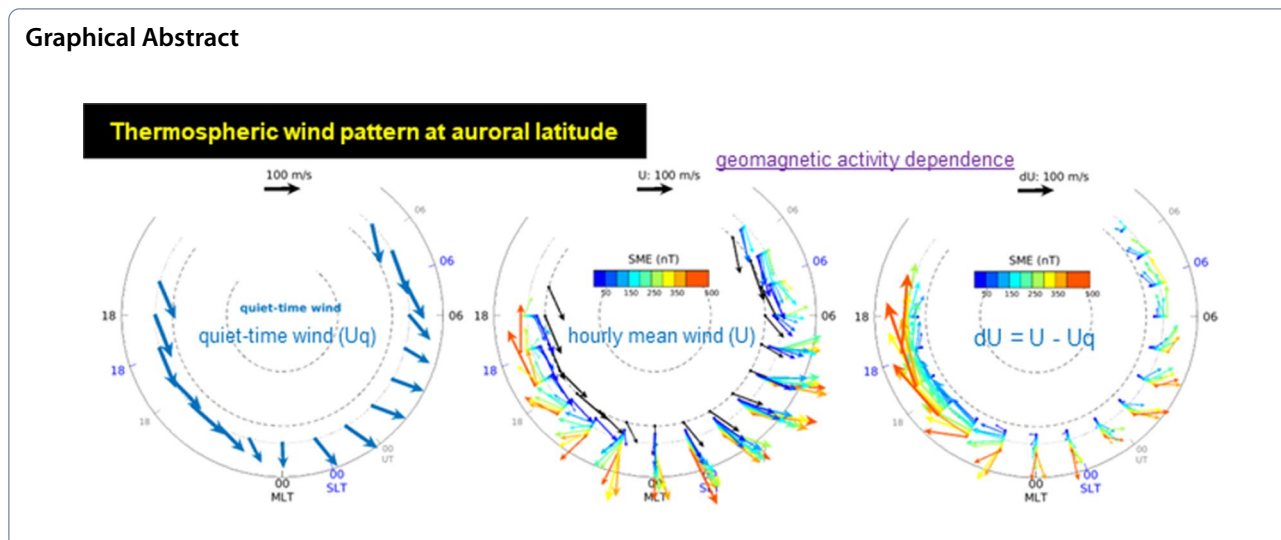
*Correspondence:
Shin-ichiro Oyama
soyama@isee.nagoya-u.ac.jp
Full list of author information is available at the end of the article

Oyama *et al. Earth, Planets and Space* (2023) 75:70

Page 2 of 13

Graphical Abstract

Introduction

Thermospheric wind dynamics at high latitudes are significantly affected by ionospheric plasma motions through particle collisions between ions and neutrals, which is known as ion drag. While ions are minor species in the upper atmosphere or partially ionized plasma, the presence of ionized gas substantially affects the thermospheric wind. The wind patterns at F-region altitudes during periods of geomagnetically quiet conditions can be represented by the pressure gradient associated with solar radiation and geostrophic force balance induced by the Coriolis and centrifugal forces. Changes in the wind pattern from the geomagnetically quiet conditions become clearer with enhancements in geomagnetic activity.

Westward ion flows in the dusk cell of an ionospheric plasma convection at auroral latitudes and the subauroral polarization streams (SAPS) induce westward acceleration of the thermospheric wind by ion drag (Conde et al. 2001; Wang et al. 2012a, b, 2018; Xu et al. 2019a). In the dawn sector, the ionospheric plasma flow at auroral latitudes is mainly eastward, but the eastward thermospheric wind is hardly seen in measurements, even during periods of high geomagnetic activity (Thayer et al. 1987; Killeen and Roble 1988; Förster et al. 2017). This is because equatorward flows are dominant in the thermosphere from midnight to dawn under a geostrophic force balance (Förster et al. 2017). In the polar cap region, both ionospheric and thermospheric flows are approximately anti-sunward. In keeping the wind streamline, the thermospheric stream crosses over the auroral latitudes in the midnight-dawn sector and transfers molecular-rich air from auroral latitudes to lower latitudes (Prölss 1993).

Statistical analyses of the ionospheric ion velocity have revealed the dawn-dusk asymmetry of the ionospheric convection pattern. This convection pattern tends to have more crescent-shaped cell at dawn and more round-shaped cell at dusk (Ruohoniemi and Greenwald 2005; Thomas and Shepherd 2018). This morphological difference may be attributed to steep gradients in the ionospheric conductivity near the solar terminator line (Atkinson and Hutchison 1978) or in the auroral zone (Vasyliunas 1970). As illustrated in previous works on the potential pattern (e.g., Ruohoniemi and Greenwald 2005; Thomas and Shepherd 2018), the horizontal potential gradient tends to be steeper at dusk than at dawn; that is, the perpendicular electric field or ion velocity at dusk tend to be larger than that at dawn. This tendency has also been substantiated by the localization of the SAPS in the dusk sector (Wang et al. 2008).

Ion drag at high latitudes leaves traces of the ion flow in the thermospheric wind field, but the level is variable because force balance with other terms depends on local time and latitude. While the ionospheric plasma flow is characterized by the dawn-dusk asymmetry in geomagnetic direction and magnitude, as mentioned above, it is still unclear how much the asymmetric ionospheric pattern is projected on the thermospheric wind pattern. While a clockwise cell-like pattern similar to dusk-side plasma convection can be found in the thermospheric wind, the cell-like structure is scarcely seen in the dawn-side thermospheric wind pattern (Fuller-Rowell et al. 1984; McCormac et al. 1985, 1987; Hernandez et al. 1990; Thayer and Killeen 1993). Reason for the asymmetric wind pattern has been interpreted being due to the pressure gradient associated with solar radiation and the geostrophic force balance rather than the effects of the ion

drag. A practical way to find the effects of the asymmetric plasma convection pattern on the thermospheric wind may be to remove the background geomagnetically quiet-time wind from the measurements. We have applied this technique in this study.

Many previous attempts have studied the geomagnetic activity dependence of the ionosphere and thermosphere by employing the Kp index to group measurements (e.g., Thayer and Killeen 1993; Emmert et al. 2006; Dhadly et al. 2017). In those analyses, Kp < 3 was widely applied to represent geomagnetically quiet conditions. However, we should note that there are many outliers with moderate levels of geomagnetic activity, even for low Kp values. Figure 1 shows the Kp dependence of the probability density function (PDF) of the SuperMAG index, SME, (Gjerloev 2012) for the period of the Fabry–Perot interferometer (FPI) measurements to be analyzed in this study (from January 23, 2009, to September 22, 2017; see "FPI measurement" section). While the method to derive the SME index is based on a same concept for the widely-used Auroral Electrojet (AE) index, it is derived from all available ground magnetometers at geomagnetic latitudes of 40–80 degrees. Number of contributing stations typically reaches approximately 110 stations, which

achieve a denser observation network than the AE index. The time resolution is 1 min, and dataset is available on the SuperMAG webpage (supermag.jhuapl.edu). The Kp level is described by individual colors, as illustrated in the box. While a large majority of measurements are taken from periods with low SME values, which are smaller than approximately 50–70 nT, there is a considerable number of measurements with moderately large SME values, even for low Kp cases. In the case of Kp < 3 (yellow), events with SME larger than 400 nT are not rare, and in some cases, the SME can exceed 800 nT. For example, ratios of events with SME larger than 200, 300, and 400 nT to events with Kp < 3 are 21.0%, 9.6% and 4.3%, respectively. Any measurements for quiet time periods defined by Kp < 3 in previous studies might have been affected by the disturbed conditions to some degree.

This study performed statistical analyses of the thermospheric wind measured with the FPI (wavelength of 630.0 nm) in Tromsø, Norway. First, the quiet time wind pattern is estimated in "Geomagnetically quiet-time wind" section. Second, the geomagnetic activity dependence of the wind pattern is derived in "Geomagnetic activity dependence of the thermospheric wind" section by grouping FPI measurements into several geomagnetic
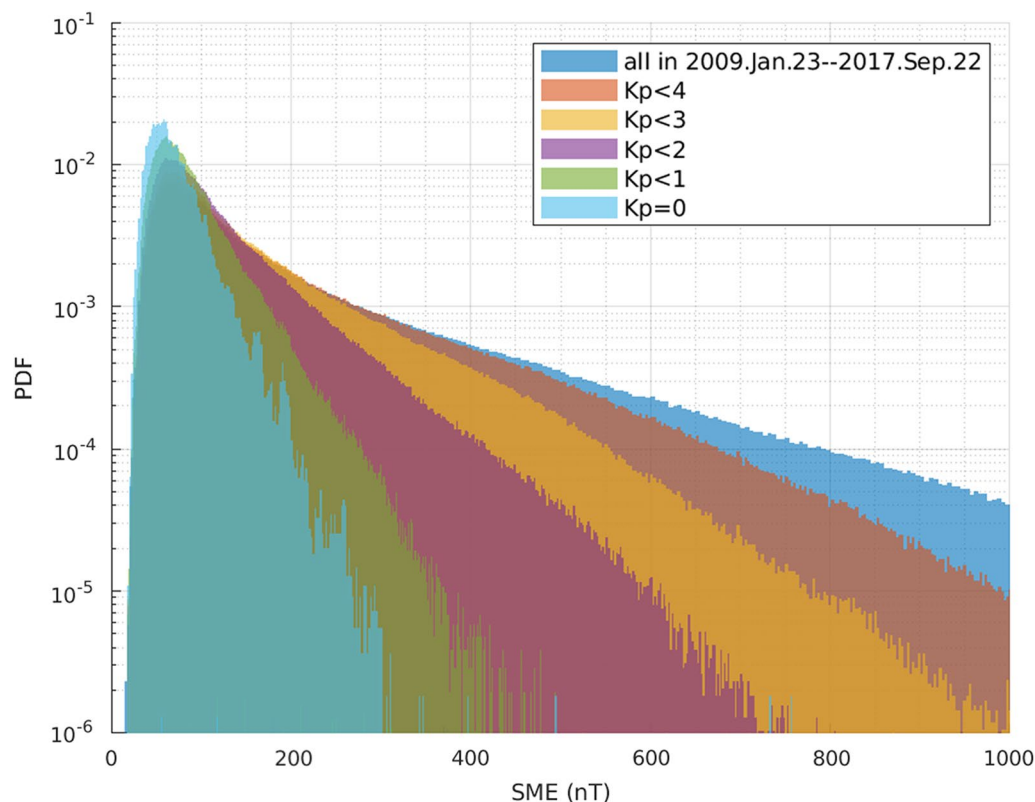

Fig. 1 Power density function (PDF) of SME from January 23, 2009 to September 22, 2017 under the Kp selection from Kp = 0 to Kp < 4. The Kp level is depicted by color as illustrated in the box

Oyama *et al. Earth, Planets and Space* (2023) 75:70

Page 4 of 13

activity levels. Deviations from the quiet-time wind are calculated for individual geomagnetic activity levels defined by the SME. In the wind deviation, a clear dawn-dusk asymmetry has been found in magnitude, which would be the first report from measurements as far as we know.

FPI Measurement

The FPI has been operated since January 2009 at the Tromsø European Incoherent Scatter (EISCAT) radar site (69.6°N and 19.2°E in geographic coordinates and 66.7°N in geomagnetic coordinates) for winter months (mainly from the middle of September to the beginning of April). Four cardinal points with a zenith angle of 45° and geographic vertical (i.e., five directions) were measured sequentially, and the optical filters were switched between 557.7 and 630.0 nm every cycle. This study analyzed measurements at 630.0 nm with an exposure time of 60 s at each position. One cycle with five directions took 315 s, including the data transfer time from the charge-coupled device (CCD) sensor to the hard disk drive. More than ten fringes can be captured simultaneously on each line-of-sight image due to the relatively wide field of view (the full width at half maximum is approximately 4°). The Doppler shift or the line-of-sight (LoS) speed is derived from individual fringes and averaged for each exposure. The statistical standard deviation in calculating the mean value is taken as the measurement uncertainty in this study. The vector wind measurement at 630.0 nm

was made every 780 s (13 min). The combination of data from the four cardinal positions provides the horizontal components of the thermospheric wind velocity under an assumption of spatiotemporal homogeneity (500 km scale and 315 s) in the wind field. A method, which is described by Shiokawa et al. (2003, 2012), is designed to cancel out the vertical wind and the etalon gap drift in deriving meridional and zonal components of the wind from a pair of north–south and east–west LoS speeds, respectively (see Additional file 1: Fig. S1). An advantage of this method is that the horizontal wind vector can be estimated without knowing the vertical wind and the etalon gap drift. Measurements under clear sky conditions were used for the analysis referring to the status of the sky condition published on the web (https://stdb2. isee.nagoya-u.ac.jp/omti/obslst.html).

Geomagnetically quiet-time wind

This section defines the quiet-time wind profile based on the FPI measurements, which will be used for further analyses in "Geomagnetic activity dependence of the thermospheric wind" section. Figure 2 presents the SME dependence of the hourly mean wind speeds. The zonal (U_e, positive in the eastward direction) and meridional (U_n, positive in the northward direction) components are illustrated by solid and dashed curves, respectively. In calculating the mean wind, the upper limit of the SME value is assigned to select the FPI measurements, illustrated by colors from dark blue for 30 nT to red for 200
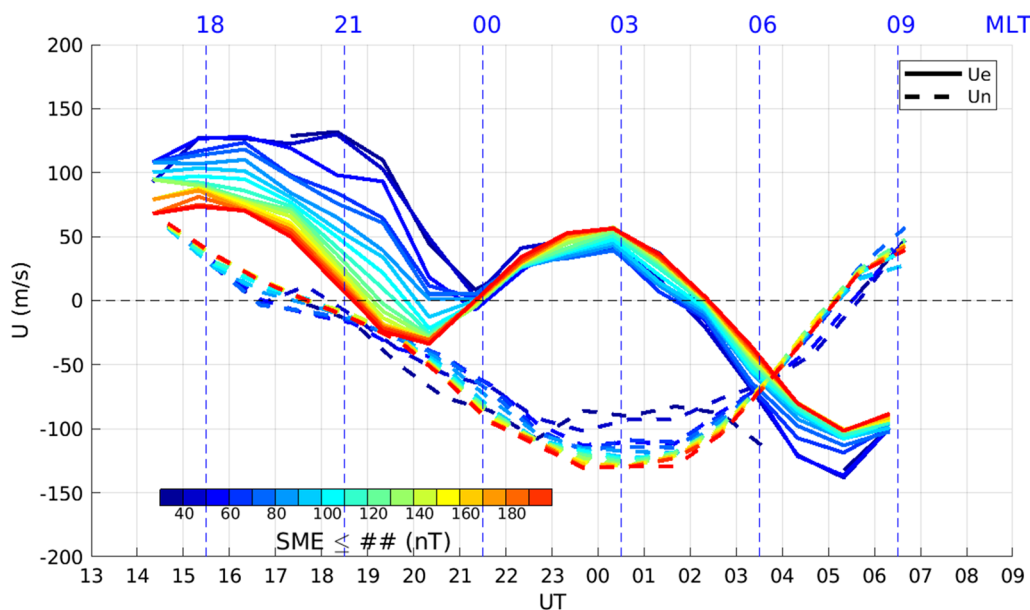

Fig. 2 Time series of the zonal (solid) and meridional (dashed) components of the mean FPI-measured wind. Colors from blue to red represent the upper limit of the SME applied to the mean wind calculation, which is incremented from 30 to 200 nT by 10 nT as depicted by a color scale in the figure. Magnetic local time (MLT) is labeled at the top bar

nT with steps of 10 nT, i.e., 18 levels in total. For example, a red curve in Fig. 2 is made of measurements with SME < 200 nT. An SME upper limit higher than 200 nT has not been employed in this calculation because there is generally less difference from the result of 200 nT with increasing limit. Magnetic local time (MLT) stamps are marked on the top. A notable feature is a gradual decrease in magnitude of the zonal component at each hour segment before 0 MLT with increasing SME upper limit. At 0 MLT, the zonal component reaches approximately 0 m/s for all SME levels, then the SME dependence turns out to be the opposite, that is, a gradual increase in the wind magnitude with increasing SME level. This pattern can be understood based on the ion drag force associated with ionospheric plasma convection, which bifurcates westward and eastward at approximately 0 MLT at auroral latitudes. In terms of the meridional wind speed, in the premidnight sector, the variations in the SME level are smaller than those for the zonal wind speed. From 0 to 6 MLT, the equatorward magnitude increases with the SME level.

For the lowest two SME cases in Fig. 2, that is, SME ≤ 30 and 40 nT, there is no notable difference in the wind pattern through the night. Since there are some gaps in the mean values for the case of SME ≤ 30 nT, we select the pattern with SME ≤ 40 nT as the geomagnetically quiet time wind in this study. The quiet-time wind in Tromsø has been studied by Xu et al. (2019a) by separating measurements with Kp ≤ 1 + and the X-component of the Tromsø magnetometer values less than 50 nT to ensure globally and locally quiet conditions, respectively. The quiet-time wind pattern (see Fig. 2 of their publication) has no significant difference from the result shown in Fig. 2 of this study (case of SME ≤ 40 nT). It is therefore considered that quality control with SME ≤ 40 nT contributes to data selection at both the global and local scales.

Figure 3 shows all available FPI measurements (gray dots) along with the quiet-time wind with an SME ≤ 40 nT (yellow circles). In terms of the meridional component (Panel a), the quiet-time wind tends to capture a part of the diurnal tide, which can be expected from the global
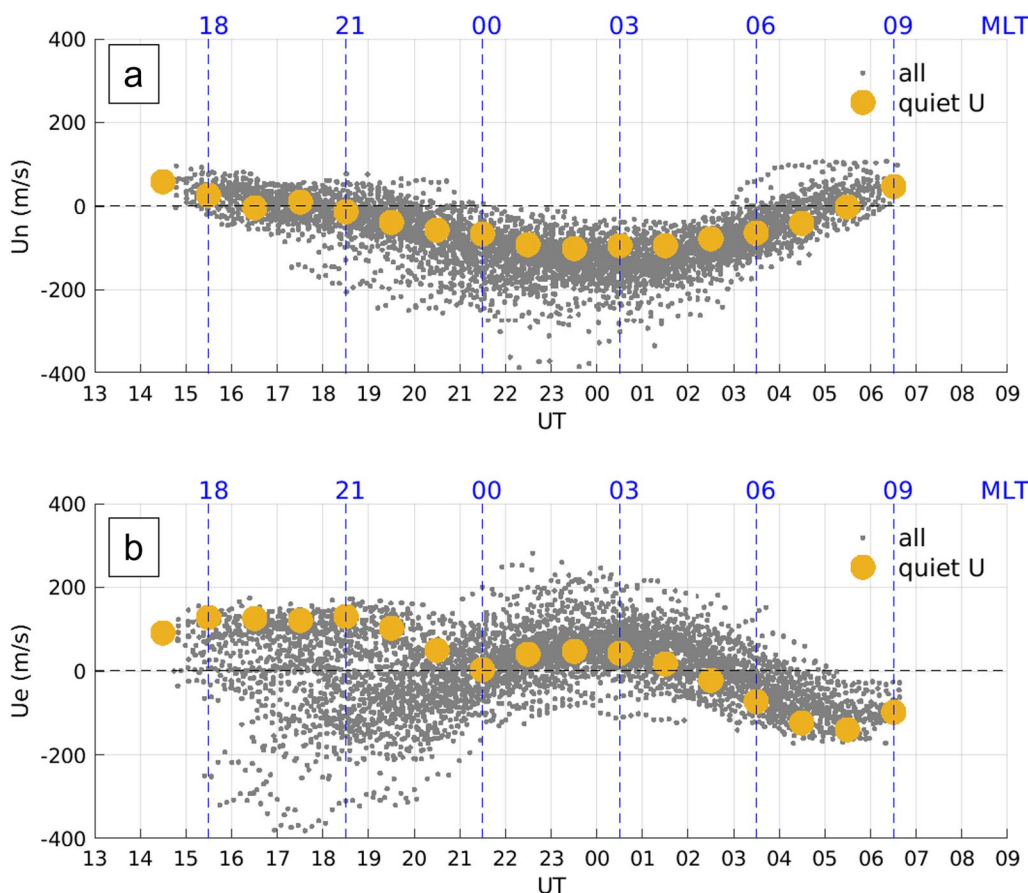

Fig. 3 Time series of the **a** meridional and **b** zonal components of all available FPI measurements (gray dots) along with the quiet-time wind, which is the same as the mean wind with SME ≤ 40 nT (yellow circles). MLT is labeled at the top bar

Oyama *et al. Earth, Planets and Space* (2023) 75:70

Page 6 of 13

pressure gradient associated with solar radiation. On the other hand, in terms of the zonal component (Panel b), the quiet-time wind before 0 MLT tends to vary following the upper envelope of the distribution. There are many measurements with large negative deviations from the quiet-time wind, reaching 500 m/s in some cases. After 0 MLT, the quiet-time zonal wind remains in the approximate the middle of the distributions but slightly

shifts westward, particularly in the late morning. The zonal deviation before 0 MLT tends to be larger than that after 0 MLT. The meridional deviation appears to peak at postmidnight.

Figure 4 presents a polar plot of the quiet-time wind vector. The MLT, solar local time (SLT) and universal time (UT) timestamps are marked in black, blue, and gray, respectively. Geomagnetic latitudes are labeled every 10° along with 66.7° of the Tromsø latitude. This wind pattern will be compared in "Discussion" section with the previous theoretical prediction and statistical results.

Geomagnetic activity dependence of the thermospheric wind

The motivation of studying the geomagnetic activity dependence of the thermospheric wind is to know how much the wind can vary by external forcing originating in the magnetosphere. In terms of this scientific objective, the hourly mean wind profiles shown in Fig. 2 may not be appropriate to achieve the goal. This is because most measurements have been obtained at low SME values, as shown in Fig. 1, and the results in Fig. 2 can be attenuated by a large majority of the quiet time measurements. To study the dependence, FPI measurements have been grouped into 9 SME bins (8 bins every 50 nT below 400 nT and one bin from 400 to 500 nT), and hourly mean winds have been calculated as shown in Fig. 5. Time series of the wind are presented separately in 9 colors from dark blue for the lowest SME bin (0–50 nT) to red
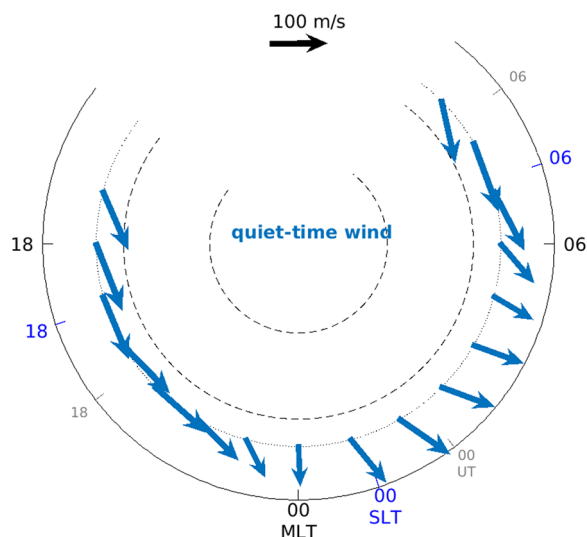

Fig. 4 Polar plot of the quiet-time wind. MLT, solar local time (SLT) and universal time (UT) are marked in black, blue, and gray, respectively. A reference vector magnitude is presented at the top
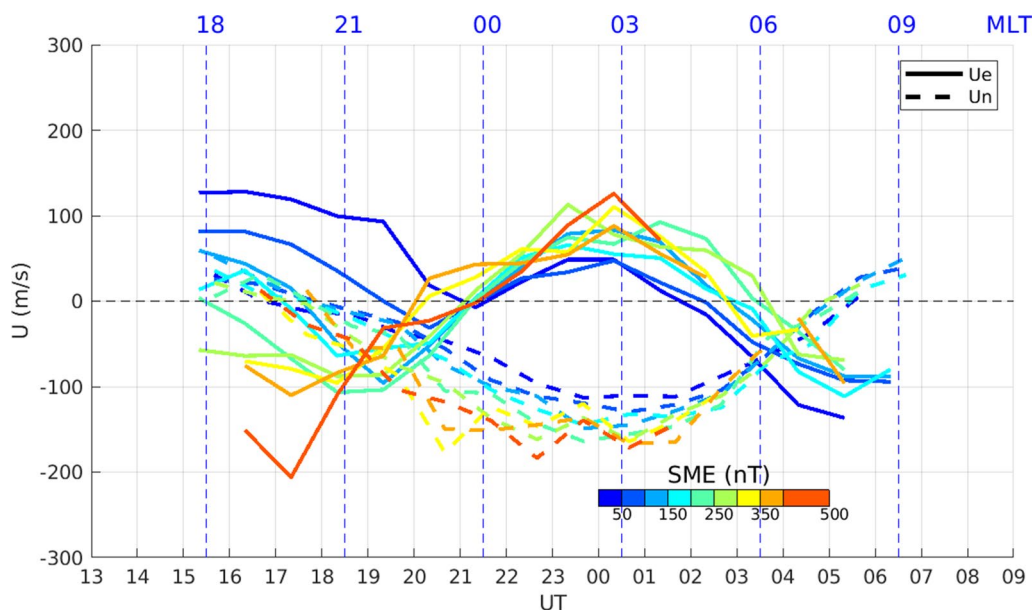

Fig. 5 Time series of the zonal (solid) and meridional (dashed) components of the mean FPI-measured wind under 9 SME levels as illustrated by individual colors. MLT is labeled at the top bar

Oyama *et al. Earth, Planets and Space* (2023) 75:70

Page 7 of 13

for the highest SME bin (400–500 nT). Zonal and meridional components are drawn as solid and dashed curves, respectively. The number of hourly data points for each SME level is displayed in Additional file 1: Fig. S2. A notable difference to the wind pattern in Fig. 2 is the zonal component in the dusk sector, which indicates a larger westward flow with increasing the SME level. The time of the westward peak seems to shift toward earlier hours with increasing SME level. This trend can be more clearly seen in Additional file 1: Fig. S2, which shows time series of the wind separately for individual SME levels.

Figure 6 presents the SME dependence of the wind deviation, which is derived by subtracting the quiet-time wind ("Geomagnetically quiet-time wind" section) from the hourly mean values shown in Fig. 5. In terms of the zonal component (dUe, solid curve), westward deviations are notable before 0 MLT and then turn eastward deviations with smaller magnitudes. In terms of the meridional component (dUn, dashed curve), southward deviations are dominant throughout the night except for the early evening and late morning. Meridional deviations are less than 100 m/s through the night, which are smaller than the zonal deviation maximum less than 320 m/s. Individual time series can be seen in Additional file 1: Fig. S2. A more detailed discussion will be provided in "Dawn-dusk asymmetry" section.

Figure 7 presents two polar plots made of (a) the hourly mean wind, shown in Fig. 5, and (b) the hourly mean wind deviation from the quiet-time pattern, shown in Fig. 6. The figure format is the same as Fig. 4 except for the colors of the wind vectors. To improve the visibility

of individual wind vectors, the start points are shifted meridionally from the Tromsø reference latitude (marked by a dotted circle at 66.7°). The quiet-time wind vector is presented in black as a reference in Panel (a), which is the same as Fig. 4. The two polar plots capture the overall features of the geomagnetic activity dependence of the thermospheric wind. For example, in Panel (a), the wind pattern in the dusk sector rotates from eastward (anti-sunward) to westward (sunward) with increasing SME, due to the increased effect of the ion drag compared to the pressure gradient force associated with the solar radiation. From midnight to dawn, the mean winds are dominated by equatorward flows, irrespective of the SME level. However, in the deviation plot (Panel b), the eastward component is also seen in the dawn sector with increasing SME, though smaller in magnitude than westward deviations in the dusk sector. This may be the first time that the clear dawn-dusk asymmetric pattern of the wind deviation and its dependence on the geomagnetic activity are presented based on observations, as far as we know. A more detailed discussion will be provided in "Dawn-dusk asymmetry"–"Wind fluctuations near midnight" sections.

Discussion

The important results from this study are twofold. One is the quiet-time wind pattern, which has been derived from measurements obtained under considerably low geomagnetic activity. This wind profile can be used as a baseline to calculate the wind deviations associated with geomagnetic activities. The other is the geomagnetic
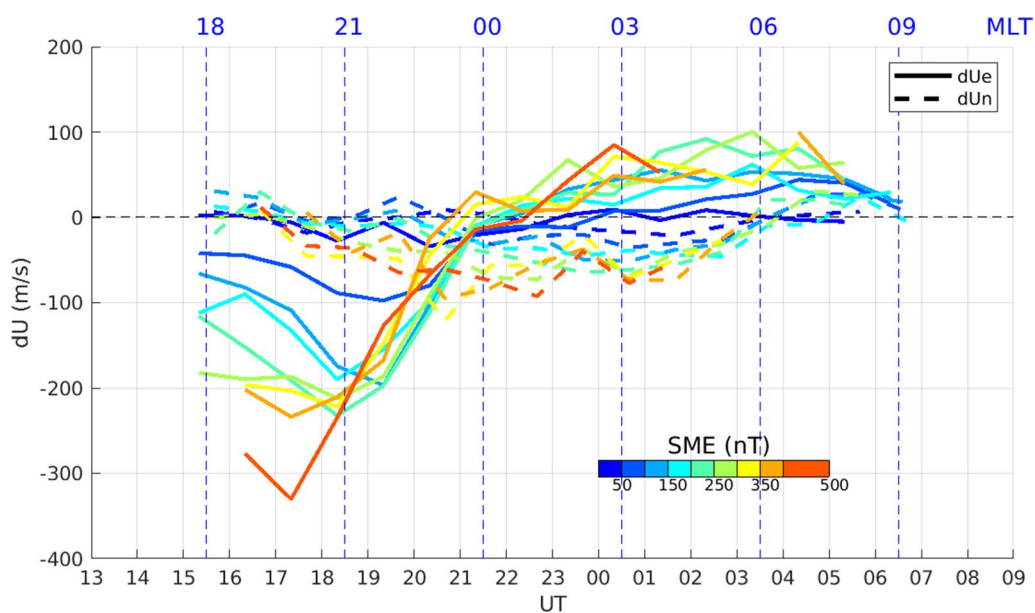

Fig. 6 Same figure format as Fig. 5 but made by dU, which was derived from deviations from the quiet-time wind
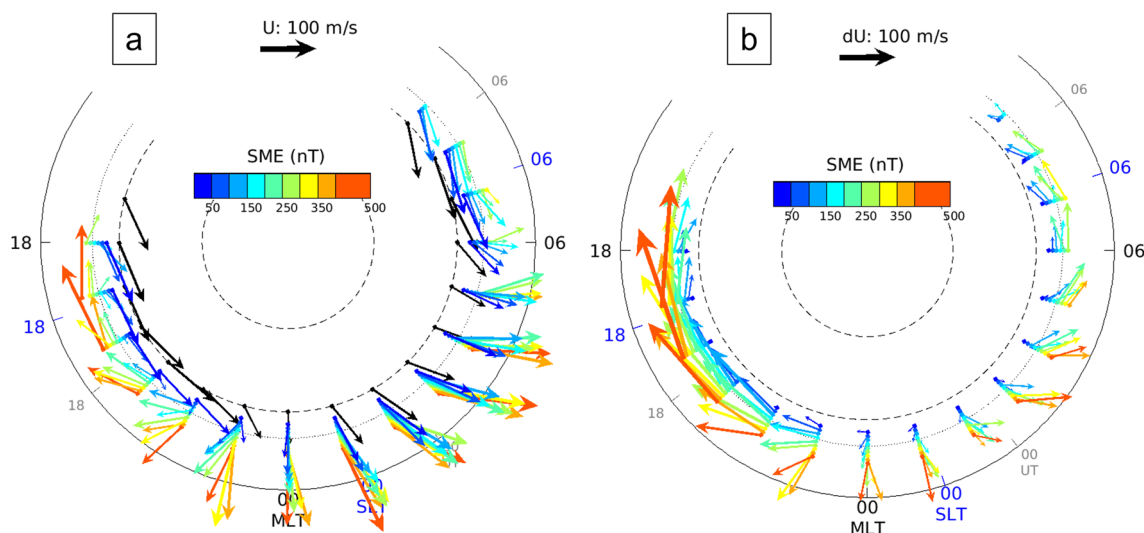
Fig. 7 Polar plot of the **a** mean wind and **b** mean deviation, which are the same values as presented in Figs. 5 and 6, respectively. The quiet-time wind vector, which is same as shown in Fig. 4, is also presented in Panel **a** in black

activity dependence of the wind and deviation from the quiet-time wind. In "Wind pattern for the period of geomagnetically quiet conditions" section, the quiet-time wind will be compared with the Horizontal Wind Model (HWM), which has been developed using data for Kp < 3 (Drob et al. 2015). In "Dawn-dusk asymmetry"–"Wind fluctuations near midnight" sections, the geomagnetic activity dependence will be compared with previous results to discuss the processes behind the wind deviation patterns.

Wind pattern for the period of geomagnetically quiet conditions
Figure 8 presents the time series of (a) meridional and (b) zonal winds from the HWM14 (Drob et al. 2015; black) and FPI measurements (blue and green curves). For reference, measurements from FPIs in Scandinavia have not been used for developing the HWM14 model (Drob et al. 2008; Drob et al. 2015). In calculating the HWM wind, the quietest 20 nights during periods of the available FPI measurement were selected, and the hourly mean values are plotted in the figure (black). The quiet-time wind, which was defined in "Geomagnetically quiet-time wind" section, is overlaid with ± 1σ (blue). A reason of the discrepancy between the two winds might be missing data of Scandinavia in the model. Hourly mean FPI winds under Kp < 3 (green curve with ± 1σ) were also overlaid in Fig. 8 to make a direct comparison with the HWM wind. In terms of the meridional component (Panel a), the three wind profiles have similar patterns, but for a few hours after 0 MLT, the FPI winds with Kp < 3 tend to be more equatorward than the HWM wind. Stronger

equatorward winds may be attributed to anti-sunward acceleration by ionospheric convection in the polar cap, which can flow into the Tromsø latitude, and to pressure gradient associated with Joule heating. On the other hand, there are significant differences in the zonal component among the three profiles. In the premidnight sector, the HWM wind (black) and FPI wind with Kp < 3 (green) deviate westward from the FPI quiet-time wind (blue). Since westward plasma flows are dominant in the premidnight ionosphere, it is considered that westward ion drag pushes the thermosphere, resulting in more westward discrepancy in the two winds. This suggests that the HWM wind may be more affected by geomagnetic activity because dataset for Kp < 3 was used in developing the HWM14 model. After reaching 0 m/s at 0 MLT for all three profiles, the eastward flow is dominant for two FPI profiles by 4–5 MLT but the westward flow remains until late morning for the HWM wind. While eastward plasma flows are expected in the dawn sector, greater eastward deviations in the FPI winds than the HWM wind at postmidnight are not due to the ion drag at auroral latitudes because hourly mean FPI zonal winds from 0 to 4 MLT remain eastward even for low SME levels (see Fig. 5). Comparing the zonal winds for the two FPI profiles in Fig. 8, the FPI wind for the Kp < 3 case (green) tends to deviate more eastward than the quiet-time wind (blue), probably resulting in the eastward ion drag in the dawn sector.

Returning to Fig. 1, which presents the PDF of the SME under several Kp levels, it may be reasonable to assume that the thermospheric wind at high latitudes can be statistically affected by geomagnetic activity
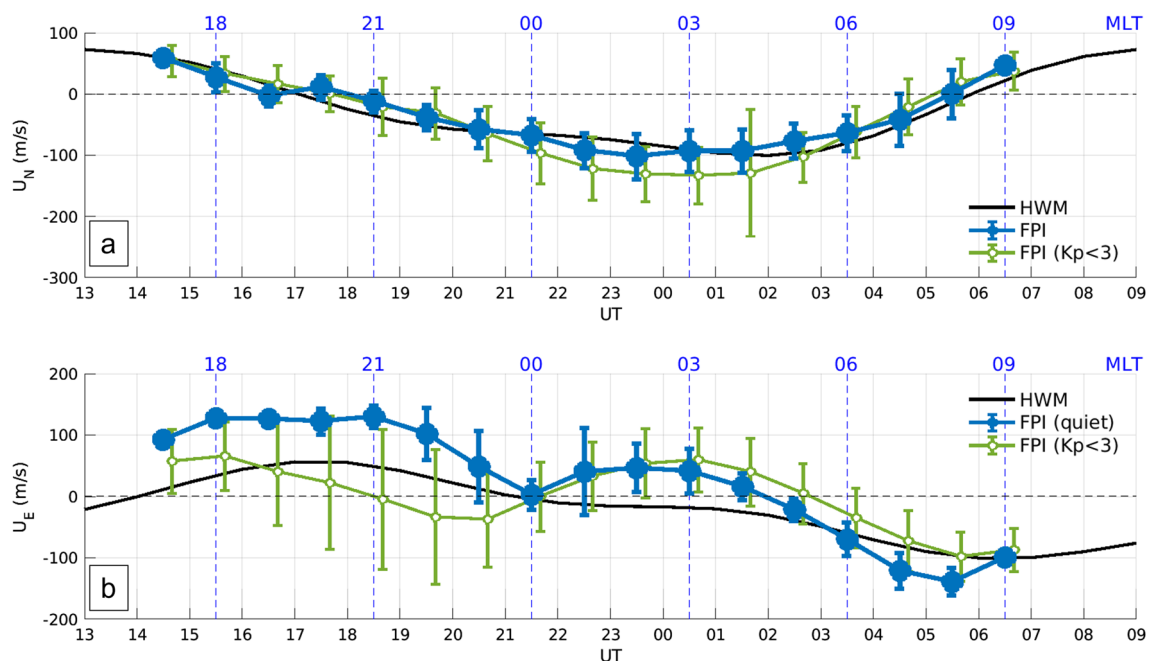
Oyama *et al. Earth, Planets and Space* (2023) 75:70

Page 9 of 13

Fig. 8 Time series of **a** meridional and **b** zonal components of the quiet-time wind (blue) derived in this study along with quiet-time HWM-modeled winds (black) and mean FPI-measured wind for Kp < 3 (green). The vertical bar represents ± 1 statistical standard deviation for individual values

even under Kp < 3, although the proportion of geomagnetically quiet event tends to increase with decreasing Kp. In previous statistical studies, a threshold of Kp < 3 has been frequently applied to group measurements (e.g., Thayer and Killeen 1993; Emmert et al. 2006; Dhadly et al. 2017). In some cases, Kp < 2 (e.g., Aruliah et al. 1999; Xiong et al. 2015; Yamazaki et al. 2015) or Kp < 4 (e.g., Wang et al. 2011; Wang and Lühr 2013; Zhang et al. 2015) have also been applied. The Kp index might have been used in these studies to characterize geomagnetic storms rather than substorms. However, thermospheric winds at high latitudes can be moderately disturbed at substorms during nonstorm periods. It would therefore be more appropriate to apply the AE or SME indices to characterize geomagnetic activity impacts.

The quiet-time wind, which was defined by SME ≤ 40 nT in this study, can be affected by some amounts of geomagnetic energy inputs. The thermospheric wind pattern without any external forcing from the magnetosphere will not be measured because the energy inputs never totally disappear. Note that "quiet-time" in this study means a period of a considerably small amount of energy input. Thermospheric winds at high latitudes may be sensitive to respond to small increases in the energy input (Oyama et al. 2022). This is evident in the westward dU at premidnight in Fig. 7b for SME < 50 nT (the northernmost dark

blue arrows), which is just a 10 nT increase from the quiet-time SME level of 40 nT.

Dawn-dusk asymmetry

A two-cell pattern is typically seen in the ionospheric convection at high latitudes, but it is not a representative feature for the thermospheric wind. Statistical analysis of the Dynamics Explorer (DE) 2 measured wind depicts a relatively clear clockwise rotation at dusk, that is, anti-sunward flow in the polar cap and westward flow at dusk at auroral latitudes, but hardly reveals a cell pattern at dawn (McCormac et al. 1985, 1987; Thayer and Killeen 1993). Statistical analysis of the Challenging Minisatellite Payload (CHAMP) accelerometer data also shows a similar dawn-dusk asymmetry (Fig. 10.3 in Förster et al. 2017). Some similarities can be captured in Fig. 7a of this study. While the dusk thermospheric wind rotates westward with geomagnetic activity, the dawn flow does not show a clear eastward turning. A unique theoretical experiment was conducted by Fuller-Rowell et al. (1984) to discern the dawn-dusk asymmetry. Figure 8 of their publication presents the trajectory of the two air parcels starting separately from dusk and dawn at 70° latitude with an initial velocity of 300 m/s westward and eastward, respectively. These directions are parallel to the return flow of the ionospheric plasma convection at each local time. The dusk side parcel keeps moving westward

for 6 h at almost the same latitude as the start, which suggests that the parcel can feel the ion drag for a long time. On the other hand, the dawn side parcel starts rotating equatorward soon after release, escaping from the auroral region, because both the Coriolis and the centrifugal forces tend to push the thermosphere equatorward. This difference in motion is attributed to the balance between the Coriolis force and the centrifugal force. In the dusk sector, the thermospheric wind can reverse direction by prolonged exposure to the westward ion drag, but in the dawn sector, the air parcel may flow away from the auroral region toward lower latitudes with little or no change in direction eastward by the ion drag. The difference between dusk and dawn is partially related to a delay time of the thermospheric response to changes in the ionospheric plasma convection, as the delay is a function of the plasma density. An inertial delay by the ion drag may vary in the range of a few 10 s min to several hours (Aruliah et al. 1999; Kosch et al. 2001).

The dawn-dusk asymmetry of the mean wind has been reported in several publications (Killeen and Roble 1988; Förster et al. 2017, and references therein). However, that of the wind deviation or dU may have not been reported as far as we know. The horizontal gradient of the ionospheric potential pattern tends to be steeper at dusk than at dawn; that is, a larger perpendicular electric field or ion velocity can be expected at dusk than at dawn (Ruohoniemi and Greenwald 2005; Förster and Haaland 2015). Since a faster plasma flow can transfer more momentum to neutral particles through collisions, it is reasonable to conclude that the dawn-dusk asymmetry of the ionospheric plasma convection contributes to the asymmetry of the thermospheric wind acceleration. This suggests that the weaker dawn cell of the thermospheric wind may be caused by not only the geostrophic force balance but also the weaker ion drag forcing at dawn, although the former process has been a focal point for the mechanism. However, we may need more analysis with quantitative comparisons between the ion velocity and wind.

Importance of the quiet-time baseline wind to understand westward wind acceleration at dusk

Earlier papers have shown that in the pre-midnight sector during the substorm growth phase winds are accelerated in the westward direction by the ion drag force, which then may change to eastward acceleration in the expansion phase of the substorm in the midnight sector (Cai et al. 2019; Xu et al. 2019b; Oyama et al. 2022). Substorm-associated wind disturbances relative to the onset are illustrated in Fig. 9 of Zou et al. (2021). The figure illustrates that, before the substorm onset, westward acceleration can be recognized poleward of the onset latitude in the premidnight sector, but at the equatorward

side of the onset latitude, westward acceleration becomes weaker in the postmidnight sector. The westward acceleration at the equatorward side of the onset latitude is developed after the onset. However, this trend seems to be inconsistent with the results of this study because westward wind deviations in this study can be seen at all hours in dusk for all SME levels (see Figs. 6, 7b). While the quiet-time wind in this study has been constructed with measurements under SME ≤ 40 nT, the quiet-time wind in Zou et al. (2021) was made including more active conditions or an AE* range of 0–100 nT (note that AE* presents the maximum AE value in the past two hours of individual measurements). As seen in Fig. 6 of this study, we can find westward deviations for the case of 50 ≤ SME < 100 nT. While SME is not exactly the same as AE, it is reasonable to assume that the quiet-time wind employed by Zou et al. (2021) would be enhanced more than that of this study.

An interesting event at dusk is time of change in the wind acceleration direction from westward to eastward. A peak of the westward dU shifts to earlier MLT with increasing SME level (Fig. 6 and Additional file 1: Fig. S2). In cases of 50 ≤ SME < 100 nT and 100 ≤ SME < 150 nT, the peak appears at 22 MLT (=19.5 UT), but it shifts 20 MLT (=17.5 UT) in the case of 400 ≤ SME < 500 nT, which is a 2-h change. Since the end time of the MLT region confining the westward acceleration at dusk may coincide with the substorm onset (Cai et al. 2019; Xu et al. 2019b; Oyama et al. 2022), wind variations relative to the substorm onset are an important target to understand the thermospheric response at high latitudes. In conducting this analysis, baseline or the quiet-time wind is an essential parameter to testify to the result.

Wind fluctuations near midnight

Measurement uncertainty, which is illustrated by the thickness of individual curves in Additional file 1: Fig. S3, is considerably smaller than the statistical standard deviation of the hourly mean wind speeds, which are marked by the vertical bar in Additional file 1: Fig. S3. It is therefore considered that wind fluctuations are real features in the thermosphere. Of particular interest is the MLT dependence, which has a tendency of larger standard deviations in the premidnight sector than in the postmidnight sector for the zonal component. This trend can be expected in Fig. 3 and confirmed by calculation with an SME bin of 100 nT (see Additional file 1: Fig. S4), which provides a larger number of measurements for individual SME bins. Since substorm growth and expansion phases are more likely to occur in the premidnight sector rather than in the postmidnight sector, thermospheric winds may fluctuate more during substorm growth and expansion phases. On the other hand, FPI measurements at the

E-region height with the auroral green line (557.7 nm) show wind fluctuations in the pulsating auroral patch at the substorm recovery phase (Oyama et al. 2010, 2016). This issue should be discussed by analyzing higher time resolution measurements in the future.

In the meridional component, equatorward dU is dominant through the night, except for the early evening and late morning hours. The magnitude slightly increases with the SME level, as shown in Fig. 6. One possible reason is acceleration in the polar cap by ion drag associated with anti-sunward plasma flows. The faster thermospheric stream likely reaches nightside auroral latitudes during periods of more active conditions. Another candidate is local thermal expansion due to Joule heating, which can also be enhanced with the SME level. For this case, in the polar cap region near the night-time auroral oval, anti-sunward thermospheric flows may be decelerated. This would be an interesting topic for future work.

Conclusions

Thermospheric winds measured with the FPI in Tromsø, Norway (69.6°N and 66.7°N in geographic and geomagnetic coordinates, respectively) in winter months for approximately 9 years (2009 January to 2017 September) were statistically analyzed by grouping data into several SME bins from 30 to 500 nT. Hourly mean values under SME $\leq$ 40 nT were defined as geomagnetic quiet-time wind in this study. The quiet-time wind pattern was compared to the HWM14 model, and clear discrepancies were depicted. We suggest that the reason is the use of Kp $<$ 3 condition in deriving the quiet-time winds in the HWM14 model, which may also include time periods with substorms and auroral electrojet enhancements.

Wind deviations or dU were derived by subtracting the quiet-time wind from the measurements. In the case of low SME levels, the thermospheric wind pattern is dominated by the pressure gradient associated with solar radiation and the geostrophic force balance. However, because of ion drag, the wind pattern can deviate toward the ionospheric plasma flow even with a small increase in the geomagnetic activity. The dU pattern is characterized by larger westward values at dusk and smaller eastward values at dawn. One of the reasons to produce asymmetry in the magnitude is likely the dawn-dusk asymmetry of the ionospheric plasma convection. This is the first study to our knowledge to report a dawn-dusk asymmetry in the thermospheric wind acceleration as well as the eastward wind acceleration at dawn by the ion drag. From midnight to dawn, equatorward winds are dominant for all SME levels but slightly increase in magnitude and rotate eastward with the SME.

Abbreviations

SAPS	Subauroral polarization stream
PDF	Probability density function
SuperMAG	Global ground-based magnetometer initiative
FPI	Fabry–Perot interferometer
SME	SuperMAG auroral electrojet index
EISCAT	European Incoherent Scatter
CCD	Charge-coupled device
MLT	Magnetic local time
SLT	Solar local time
UT	Universal time
dU	Wind deviation from the quiet-time wind
dUe, dUn	Zonal and meridional component of the wind deviation
HWM	Horizontal wind model
AE	Auroral electrojet index
DE	Dynamics explorer
CHAMP	Challenging minisatellite payload
FUV	Far ultraviolet
TEC	Total electron content
TIMEGCM	Thermosphere ionosphere mesosphere electrodynamics general circulation model
IMF	Interplanetary magnetic field

Supplementary Information

The online version contains supplementary material available at https://doi.org/10.1186/s40623-023-01829-0.

Additional file 1. Additional Figures: Figures A1–A4.

Declarations

Ethics approval and consent to participate
Not applicable.

Consent for publication
Not applicable.

Competing interests
There are no financial and non-financial competing interests for this work.

Author details
[1]Institute for Space-Earth Environmental Research, Nagoya University, Nagoya, Japan. [2]National Institute of Polar Research, Tachikawa, Japan. [3]Space Physics and Astronomy Research Unit, University of Oulu, Oulu, Finland. [4]Graduate School of Science Planetary Plasma and Atmospheric Research Center, Tohoku

Oyama *et al. Earth, Planets and Space* (2023) 75:70

Page 12 of 13

University, Sendai, Japan. [5]Department of Computer and Network Engineering, The University of Electro-Communications, Chofu, Japan.

References

Aruliah AL, Muller-Wodarg ICF, Schoendorf J (1999) Consequences of geomagnetic history on the high-latitude thermosphere and ionosphere: averages. J Geophys Res 104(A12):28073–28088. https://doi.org/10.1029/1999JA900334

Atkinson G, Hutchison D (1978) Effect of the day night ionospheric conductivity gradient on polar cap convective flow. J Geophys Res 83(A2):725–729. https://doi.org/10.1029/JA083iA02p00725

Cai L, Oyama S-I, Aikio A, Vanhamäki H, Virtanen I (2019) Fabry–Perot interferometer observations of thermospheric horizontal winds during magnetospheric substorms. J Geophys Res Space Phys 124:3709–3728. https://doi.org/10.1029/2018JA026241

Conde M et al (2001) Assimilated observations of thermospheric winds, the aurora, and ionospheric currents over Alaska. J Geophys Res 106(A6):10493–10508. https://doi.org/10.1029/2000JA000135

Dhadly M, Emmert J, Drob D, Conde M, Doornbos E, Shepherd G, Makela J, Wu Q, Niciejewski R, Ridley A (2017) Seasonal dependence of northern high-latitude upper thermospheric winds: a quiet time climatological study based on ground-based and space-based measurements. J Geophys Res Space Phys 122:2619–2644. https://doi.org/10.1002/2016JA023688

Drob DP et al (2008) An empirical model of the Earth's horizontal wind fields: HWM07. J Geophys Res 113:A12304. https://doi.org/10.1029/2008JA013668

Drob DP et al (2015) An update to the horizontal wind model (HWM): the quiet time thermosphere. Earth Space Sci 2:301–319. https://doi.org/10.1002/2014EA000089

Emmert JT, Faivre ML, Hernandez G, Jarvis MJ, Meriwether JW, Niciejewski RJ, Sipler DP, Tepley CA (2006) Climatologies of nighttime upper thermospheric winds measured by ground-based Fabry–Perot interferometers during geomagnetically quiet conditions: 1. Local time, latitudinal, seasonal, and solar cycle dependence. J Geophys Res 111:A12302. https://doi.org/10.1029/2006JA011948

Förster M, Haaland S (2015) Interhemispheric differences in ionospheric convection: cluster EDI observations revisited. J Geophys Res Space Phys 120:5805–5823. https://doi.org/10.1002/2014JA020774

Förster M, Doornbos E, Haaland S (2017) The role of the upper atmosphere for dawn-dusk differences in the coupled magnetosphere–ionosphere–thermosphere system. Dawn-dusk asymmetries in planetary plasma environments. Geophys Monogr 230:125–141

Fuller-Rowell TJ, Rees D, Quegan S, Bailey GJ, Moffett RJ (1984) The effect of realistic conductivities on the high-latitude neutral thermospheric circulation. Planet Space Sci 32(4):469–480. https://doi.org/10.1016/0032-0633(84)90126-0

Gjerloev JW (2012) The SuperMAG data processing technique. J Geophys Res 117:A09213. https://doi.org/10.1029/2012JA017683

Hernandez G, Smith RW, Roble RG, Gress J, Clark KC (1990) Thermospheric dynamics at the south pole. Geophys Res Lett 17:1255

Killeen TL, Roble RG (1988) Thermosphere dynamics: contributions from the first 5 years of the dynamics explorer program. Rev Geophys 26(2):329–367. https://doi.org/10.1029/RG026i002p00329

Kosch MJ, Cierpka K, Rietveld MT, Hagfors T, Schlegel K (2001) High-latitude ground-based observations of the thermospheric ion-drag time constant. Geophys Res Lett 28:1395–1398. https://doi.org/10.1029/2000GL012380

McCormac FG, Killeen TL, Gombosi E, Hays PB, Spencer NW (1985) Configuration of the high-latitude thermosphere neutral circulation for IMF BY negative and positive. J Geophys Res 12:155–158

McCormac FG, Killeen TL, Thayer JP, Hernandez G, Tschan CR, Ponthieu J-J, Spencer NW (1987) Circulation of the polar thermosphere during geomagnetically quiet and active times as observed by dynamics explorer 2. J Geophys Res 92(A9):10133–10139. https://doi.org/10.1029/JA092iA09p10133

Oyama S, Shiokawa K, Kurihara J, Tsuda TT, Nozawa S, Ogawa Y, Otsuka Y, Watkins BJ (2010) Lower-thermospheric wind fluctuations measured with an FPI during pulsating aurora at Tromsø, Norway. Ann Geophys 28:1847–1857. https://doi.org/10.5194/angeo-28-1847-2010

Oyama S, Shiokawa K, Miyoshi Y, Hosokawa K, Watkins BJ, Kurihara J, Tsuda TT, Fallen CT (2016) Lower thermospheric wind variations in auroral patches during the substorm recovery phase. J Geophys Res Space Phys 121:3564–3577. https://doi.org/10.1002/2015JA022129

Oyama S, Vanhamäki H, Cai L, Aikio A, Rietveld M, Ogawa Y, Raita T, Kellinsalmi M, Kauristie K, Kozelov B, Shinbori A, Shiokawa K, Tsuda TT, Sakanoi T (2022) Thermospheric wind response to ionospheric variations in the trough: event at a pseudo breakup during geomagnetically quiet conditions. Earth Planets Space 74:154. https://doi.org/10.1186/s40623-022-01710-6

Prölss GW (1993) On explaining the local time variation of ionospheric storm effects. Ann Geophys 11:1–9

Ruohoniemi JM, Greenwald RA (2005) Dependencies of high-latitude plasma convection: consideration of interplanetary magnetic field, seasonal, and universal time factors in statistical patterns. J Geophys Res 110:A09204. https://doi.org/10.1029/2004JA010815

Shiokawa K, Otsuka Y, Oyama S et al (2012) Development of low-cost sky-scanning Fabry–Perot interferometers for airglow and auroral studies. Earth Planet Sp 64:1033–1046. https://doi.org/10.5047/eps.2012.05.004

Shiokawa K, Kadota T, Otsuka Y, Ogawa T, Nakamura T, Fukao S (2003) A two-channel Fabry–Perot interferometer with thermoelectric-cooled CCD detectors for neutral wind measurement in the upper atmosphere. Earth Planets Space 55:271–275. https://doi.org/10.1186/BF03351759

Thayer JP, Killeen TL, McCormac FG, Tschan CR, Ponthieu JJ, Spencer NW (1987) Thermospheric neutral wind signatures dependent on the east-west component of the interplanetary magnetic field for Northern and Southern Hemispheres as measured from Dynamics Explorer 2. Ann Geophys Ser A 5:363–368

Thayer JP, Killeen TL (1993) A kinematic analysis of the high-latitude thermospheric neutral circulation pattern. J Geophys Res 98(A7):11549–11565. https://doi.org/10.1029/93JA00629

Thomas EG, Shepherd SG (2018) Statistical patterns of ionospheric convection derived from mid-latitude, high-latitude, and polar SuperDARN HF radar observations. J Geophys Res Space Phys 123:3196–3216. https://doi.org/10.1002/2018JA025280

Vasyliunas VM (1970) Mathematical models of magnetospheric convection and its coupling to the ionosphere. In: McCormac BM (eds) Particles and fields in the magnetosphere. Astrophysics and space science library, vol 17. Springer, Dordrecht. https://doi.org/10.1007/978-94-010-3284-1_6

Wang H, Lühr H (2013) Seasonal variation of the ion upflow in the topside ionosphere during SAPS (subauroral polarization stream) periods. Ann Geophys 31:1521–1534. https://doi.org/10.5194/angeo-31-1521-2013

Wang H, Ridley AJ, Lühr H, Liemohn MW, Ma SY (2008) Statistical study of the subauroral polarization stream: its dependence on the cross–polar cap potential and subauroral conductance. J Geophys Res 113:A12311. https://doi.org/10.1029/2008JA013529

Wang H, Lühr H, Häusler K, Ritter P (2011) Effect of subauroral polarization streams on the thermosphere: a statistical study. J Geophys Res 116:A03312. https://doi.org/10.1029/2010JA016236

Wang H, Lühr H, Ritter P, Kervalishvili G (2012a) Temporal and spatial effects of subauroral polarization streams on the thermospheric dynamics. J Geophys Res 117:A11307. https://doi.org/10.1029/2012JA018067

Wang H, Lühr H, Ma SY (2012b) The relation between subauroral polarization streams, westward ion fluxes, and zonal wind: seasonal and hemispheric variations. J Geophys Res 117:A04323. https://doi.org/10.1029/2011JA017378

Wang H, Zhang K, Zheng Z, Ridley AJ (2018) The effect of subauroral polarization streams on the mid-latitude thermospheric disturbance neutral winds: a universal time effect. Ann Geophys 36(2):509–525

Xiong C, Lühr H, Fejer BG (2015) Global features of the disturbance winds during storm time deduced from CHAMP observations. J Geophys Res Space Phys 120:5137–5150. https://doi.org/10.1002/2015JA021302

Xu H, Shiokawa K, Oyama S, Nozawa S (2019a) High-latitude thermospheric wind study using a Fabry-Perot interferometer at Tromsø in Norway: averages and variations during quiet times. Earth Planets Space 71:110. https://doi.org/10.1186/s40623-019-1093-8

Oyama *et al. Earth, Planets and Space*   (2023) 75:70

Page 13 of 13

Xu H, Shiokawa K, Oyama Si et al (2019b) Thermospheric wind variations observed by a Fabry–Perot interferometer at Tromsø, Norway, at substorm onsets. Earth Planets Space 71:93. https://doi.org/10.1186/s40623-019-1072-0

Yamazaki Y, Kosch MJ, Sutton EK (2015) North-south asymmetry of the high-latitude thermospheric density: IMF BY effect. Geophys Res Lett 42:225–232. https://doi.org/10.1002/2014GL062748

Zhang X-X, He F, Wang W, Chen B (2015) Hemispheric asymmetry of subauroral ion drifts: Statistical results. J Geophys Res Space Phys 120:4544–4554. https://doi.org/10.1002/2015JA021016

Zou Y, Lyons L, Conde M, Varney R, Angelopoulos V, Mende S (2021) Effects of substorms on high-latitude upper thermospheric winds. J Geophys Res Space Phys 126:e2020JA028193. https://doi.org/10.1029/2020JA028193

Publisher's Note

Springer Nature remains neutral with regard to jurisdictional claims in published maps and institutional affiliations.